ACS Catalysis

Research Article

pubs.acs.org/acscatalysis

Computational Insights on an Artificial Imine Reductase Based on the Biotin−Streptavidin Technology

Victor Muñoz Robles,[†] Pietro Vidossich,[†] Agustí Lledós,[†] Thomas R. Ward,[⊥] and Jean-Didier Maréchal*[,†]

[†]Departament de Química, Universitat Autònoma de Barcelona, Edifici C.n., 08193 Cerdanyola del Vallés, Barcelona, Spain.
[⊥]Department of Chemistry, University of Basel, Spitalstrasse 51, CH-4056 Basel, Switzerland.

Supporting Information

ABSTRACT: We present a computational study that combines protein−ligand docking, quantum mechanical, and quantum mechanical/molecular mechanical calculations to scrutinize the mechanistic behavior of the first artificial enzyme able to enantioselectively reduce cyclic imines. We applied a novel strategy that allows the characterization of transition state structures in the protein host and their associated reaction paths. Of the most striking results of our investigation is the identification of major conformational differences between the transition state geometries of the lowest energy paths leading to (*R*)- and (*S*)-reduction products. The molecular features of (*R*)- and (*S*)-transition states highlight distinctive patterns of hydrophobic and polar complementarities between the substrate and the binding site. These differences lead to an activation energy gap that stands in very good agreement with the experimentally determined enantioselectivity. This study sheds light on the mechanism by which transfer hydrogenases operate and illustrates how the change of environment (from homogeneous solution conditions to the asymmetric protein frame) affect the reactivity of the organometallic cofactor. It provides novel insights on the complexity in integrating unnatural organometallic compounds into biological scaffolds. The modeling strategy that we pursued, based on the generation of "pseudo transition state" structures, is computationally efficient and suitable for the discovery and optimization of artificial enzymes. Alternatively, this approach can be applied on systems for which a large conformational sampling is needed to identify relevant transition states.

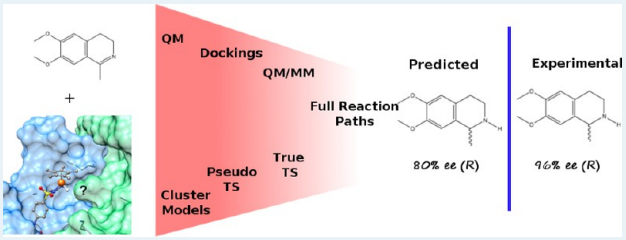

KEYWORDS: *artificial enzymes, asymmetric catalysis, imine reduction, computational chemistry, QM/MM, protein−ligand dockings*

INTRODUCTION

Artificial enzymes which result from the incorporation of a catalytically competent metal cofactor within a protein environment, are attracting attention as alternatives to more-traditional homogeneous and enzymatic catalysts.[1−5]

Several complementary strategies to create non-natural enzymes have been pursued, with varying degrees of success.[6−9] As generating catalytic function ex nihilo remains challenging, a promising approach consists of the incorporation of a catalytically competent moiety within a biomolecular environment (protein or oligonucleotide).[10] These hybrids, in essence, follow the conceptual framework of natural metaloenzymes: the cofactor, including its first coordination sphere, by and large dictates the catalytic activity, while the protein, which provides the second coordination sphere environment, controls substrate selectivity.[11] Within this framework, the choice of macromolecular scaffold dictates the anchoring strategy (i.e., dative,[12] covalent,[13] or supramolecular,[8,14]) whereby the artificial cofactor determines which transformation can be catalyzed.[5−9] Since the selected macromolecular host was not optimized by nature to accommodate the artificial cofactor or to catalyze the transformation considered, genetic optimization offers nearly limitless opportunities to improve the catalytic performance of artificial metaloenzymes.

Inspired by a visionary report by Whitesides in 1978,[15] the Ward group and others have been pursuing the biotin-(strept)avidin technology to create artificial metaloenzymes.[7,15−19] Following this supramolecular anchoring strategy, the introduction of a biotinylated organometallic moiety within streptavidin (STREP) affords artificial metaloenzymes for a variety of transformations, including hydrogenation, allylic alkylation, metathesis, C−H activation, alcohol oxidation, sulfoxidation, dihydroxylation, and transfer hydrogenation.[7,10,20−23] These designs take advantage of the high affinity of STREP for its natural ligand biotin ($K_M \approx 10^{-13}$ M). The structure of STREP is best described as a homotetrameric eight-stranded β-barrel with two close-lying biotin-binding sites. It is generally accepted that biotin-binding events are noncooperative.[24] In the context of asymmetric transfer hydrogenation, we have relied on the introduction of a biotin anchor on a Noyori-type aminosulfonamide-bearing d^6-pianostool moiety. In the presence of STREP, the biotinylated pianostool is quantitatively incorporated in the bowl-shaped biotin-binding vestibule STREP (Figure 1). Following promising results obtained for the enantioselective reduction of

Received: October 14, 2013
Revised: December 11, 2013
Published: January 22, 2014

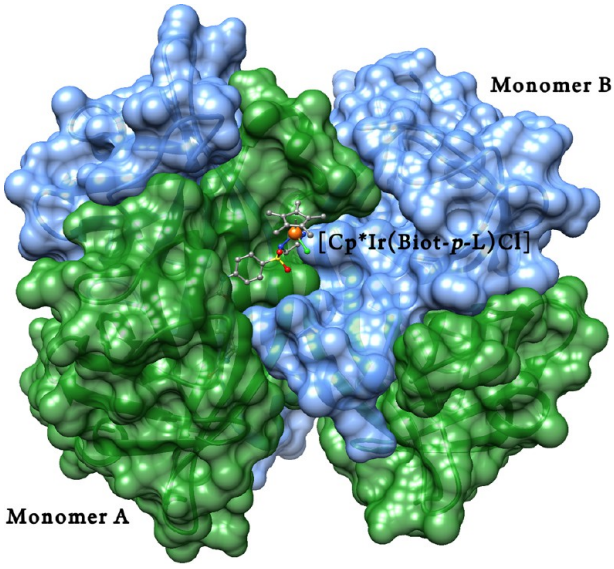

Figure 1. Cartoon picture of the tetrameric structure of S112A determined by X-ray crystallography (pdb code 3PK2). The protein is a dimer of dimers, with the cofactor binding sites of monomers A and B (green and blue ribbons and van der Waals surfaces, respectively) facing each other. The cofactor (*S*)-[Cp*Ir(Biot-*p*-L)Cl] is shown in a ball-and-stick arrangement.

ketones[14] and enones,[25] Ward and co-workers recently reported on the asymmetric transfer hydrogenation (ATH) of cyclic imines. In this context, encapsulation of [Cp*Ir(Biot-*p*-L)Cl] in STREP was most effective.[10] Site directed mutagenesis at position S112 proved particularly versatile to optimize enantioselectivity: mutant S112A affords (*R*)-salsolidine in 96% *ee*, while S112K yields (*S*)-salsolidine in 78% *ee*. These findings suggest that the transition states leading to the enantiomeric products are significantly influenced by the second coordinate sphere of the metal. The scope of this work is to pinpoint these molecular interactions.

The X-ray structure of [Cp*Ir(Biot-*p*-L)Cl]⊂S112A reveals the location of the pianostool moiety within the bowl-shaped biotin-binding vestibule of STREP, with the biotin anchor firmly locked into its natural location (Figure 1). The crystallographic data uncovers an Ir-(*S*)-configured [Cp*Ir(Biot-*p*-L)Cl] lying at the interface between two monomers (Figure 1). Based on this structural insight, an additional mutation at position K121 highlighted the importance of this residue in the enantioselection mechanism: for [Cp*Ir(Biot-*p*-L)Cl]⊂S112A-K121T, (*R*)-salsolidine is produced in only 52% *ee*.

Despite a unified view of the enantioselection mechanism for the reduction of prochiral ketones by "Noyori-type" d^6-pianostool complexes,[26] the reduction of imines proceeds via a distinct mechanism. Indeed, for a given enantiopure catalyst, e.g., [Cp*Ir{(*R*,*R*)-Tos-dpen(*p*-tolylsulfonamido-diphenylethylenediamine))}H], the (*R*)-alcohol instead of the (*S*)-imine is produced.[27] Thus, the widely accepted outersphere, synchronous, C−H···π interaction mechanism, which is valid for ketone reduction, cannot be operative for the imine transformation. Recent experimental and modeling studies suggest that the imine reduction proceeds via a iminium intermediate and thus the proton and hydride transfer are asynchronous.[26−33] Additional computations by Václavík et al. highlight the importance of an interaction between the SO_2 moiety and the N−H^+ of the substrate.[31]

Computational tools have long been expected to actively contribute to the development of artificial enzymes; the exploration of both genetic and chemical dimensions is far too diverse to perform exhaustive experiments. Undoubtedly, the two most representative successes in the field of de novo computer-aided design of artificial enzymes are the algorithms developed by the Baker group[6,34,35] and the Mayo group.[36−39] Both Baker and Mayo groups mimic a given transition state within a protein scaffold. For this purpose, they rely on a search algorithm (and on an inverse Rotameric Library, in the case of Baker) to identify protein structures that could accommodate the transition state. The best match is mutated in silico to obtain the putative active site. Further fine-tuning is achieved experimentally either by site-directed mutagenesis or by directed evolution. None of these approaches rely on QM/MM performed to compute protein-embedded transition states. However, this variable may be a key element in improving the actual in silico framework of enzyme design in particular for optimization purposes.[40] Other computational approaches to generate or optimize novel enzymes from scratch are scarce.[9,39] To the best of our knowledge, two computational studies have been reported to date on artificial metaloenzymes resulting from anchoring an artificial cofactor within a protein scaffold.[11,41] Recently, we showed that integration of quantum mechanical calculations, protein−ligand docking, and QM/MM calculations could reliably predict the localization of homogeneous catalysts into a protein host.[11] Morokuma and co-workers showed that quantum mechanical calculations could be particularly useful in characterizing the mechanism of artificial metaloenzymes, relying on the gas phase mechanism as a starting point for QM/MM calculations.[41] The authors identified that a substantial conformational change of the organometallic moiety needs to occur between the initial X-ray structure and the reactive one. However, to our knowledge, the rationalization of enantioselectivity trends in artificial metaloenzymes has yet to be achieved.

The present study aims at (i) scrutinizing the mechanism of cyclic imine transfer hydrogenation catalyzed by [CpIr(Biot-*p*-L)Cl]⊂S112A and (ii) rationalizing the origin of enantioselectivity. To do so, we use an integrative multilevel computational strategy to identify the lowest transition paths leading to an (*R*)- and (*S*)-imine reduction product: salsolidine.

MATERIALS AND METHODS

Computational Strategy. The large number of mechanistic uncertainties pertaining to the reduction of imines by a "Noyori-type" catalyst challenges the identification of the transition state structures in an artificial imine reductase. To address this, we designed a protocol combining complementary computational approaches to reduce the size of conformational and chemical space to explore (Scheme 1).

First, each mechanism put forward to date for the asymmetric transfer hydrogenation of imines was tested on a cluster composed of a reduced model of the enantiopure [Cp*Ir(Biot-*p*-L)H] and the prochiral substrate: 1-methyl-6,7-dimethoxy-3,4-dihydroisoquinoline (Scheme 2). Both the hydride attack on the *re* and *si* faces of the substrate were taken into account. Transition state structures of the lowest energy paths were subsequently used to guide protein−ligand docking simulation. Since the protein environment can substantially impact the stability of the transition state of the

dx.doi.org/10.1021/cs400921n | ACS Catal. 2014, 4, 833−842

Scheme 1. Integrative Computational Protocol

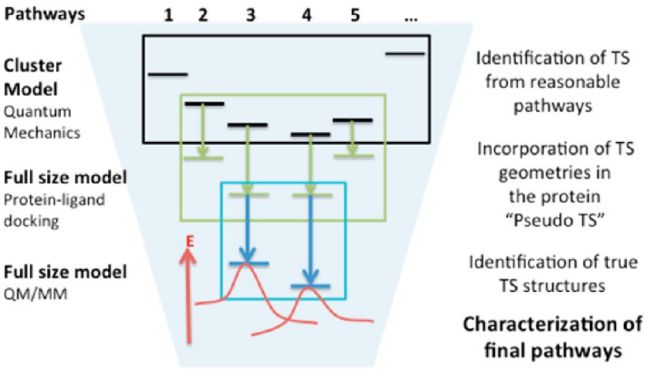

Scheme 2. Atomic Numbering Scheme for the Structures Used in This Study: (a) Simplified (*R*)-[Cp*Ir(Biot-*p*-L)H] Catalyst, (b) 1-Methyl-6,7-dimethoxy-3,4-dihydroisoquinoline, Salsolidine Precursor, (c) Hydronium Ion, and (d) Protonated Lysine Side Chain.

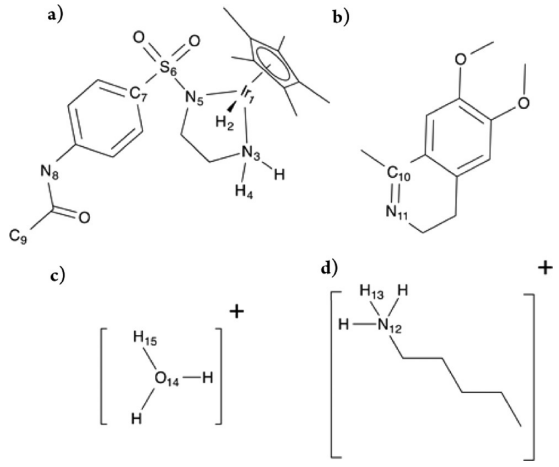

reaction, those with differences in energy smaller than 10 kcal mol^{-1} were docked in the protein. The interaction energy between these pseudo transition state structures and the protein were analyzed and the docked structures with poor predicted affinities were discarded. The remaining pseudo transition state structures were subsequently relaxed using QM/MM calculations and true transition state structures were identified. The resulting pathways are discussed in light of computed vs measured enantiomeric excess and other experimental data. This strategy shares common grounds with the recent works of Himo, and Reetz and Thiel. Himo and co-workers successfully interpreted from pure quantum mechanical models the enantioselective control of a limonene epoxide hydrolase (LEH).[42] Reetz, Thiel, and co-workers rationalized the molecular events behind the changes on the *ee* profile of various mutants of the cyclohexanone monooxygenase, using a combination of MM and QM approaches (including hybrid QM/MM methodologies).[43,44] Moreover, the joint efforts of Reetz and Thiel groups also demonstrated that MM techniques, and more specifically MD simulations, can be of great help in elucidating the effects of single-point mutations on the *ee* profile of enzymes.[45,46] In our case, the lack of information on catalytically consistent orientations of the substrate and the homogeneous catalyst in [Cp*Ir(Biot-*p*-L)Cl]⊂S112A requires a large conformational space exploration that is only affordable under a protein−ligand docking scheme.

Study of the ATH Activity of Isolated [Cp*Ir(Biot-*p*-L)H]. The lack of consensus regarding the reduction of imine by homogeneous "Noyori-type" catalysts prompted us to consider several catalytic pathways relying on cluster models of the artificial cofactor. Different modes of interaction between the substrate and the second coordination sphere around the metal were explored. Furthermore, the nature of the proton source considered (protons transferred from (i) the Ir-bound amine moiety of the ligand, (ii) the aqueous medium, or (iii) the close-lying K121 residue). Both synchronous and asynchronous delivery of hydride and protons were tested.

The cluster model includes the biotinilated catalyst up to the amide bond, the substrate and, eventually, an additional amino-acid side chain (a mimic of K121) or protonated water molecule acting as proton donors to the imine nitrogen (Scheme 2).[10] Three different mechanisms were considered (see Scheme 3).

Scheme 3. Schematic Representation of the ATH Mechanisms Considered in This Study: (a) H^-_{Ir}/H^+_{Ir}, (b) H^-_{Ir}/H^+_{Lys}, and (c) H^-_{Ir}/H^+_{Med}

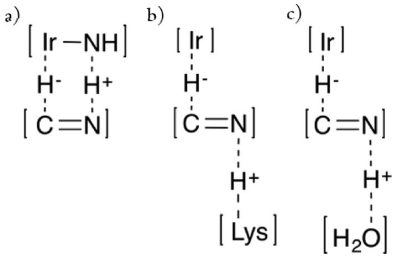

In the first one, both the hydride and the proton are transferred from the catalyst, reminiscent of the ATH of ketones (abbreviated H^-_{Ir}/H^+_{Ir}; see Scheme 3). The other two mechanisms are asynchronous, whereby the imine is protonated either by a lysine residue (abbreviated H^-_{Ir}/H^+_{Lys}, Scheme 3) or hydronium (abbreviated H^-_{Ir}/H^+_{med}, Scheme 3).[31,32] In all calculations, the Ir1···H2 distance was used as reaction coordinate for the transfer of the hydride, while the N12···H13 distance was used for the proton transfer in the models implying the lysine (Scheme 1).

Calculations were performed within the Kohn−Sham approach to density functional theory (DFT), using the PBE functional[47,48] as implemented in Gaussian09.[49] The basis set Def2-TZVPP[50] and its associated pseudopotential was used for the iridium and the 6-31G*[51] basis set for the rest of the atoms. All optimizations were carried out in water as the solvent, using a polarizable continuum model (CPCM),[52−55] as implemented in Gaussian09. The accuracy of transition states was checked by frequency analysis performed at the same level of theory. From the frequency analysis, the Gibbs energy values were obtained at 298 K.

Docking of the Pseudo Transition State Structures. Pseudo transition states are generated along the workflow by docking the transition state structures obtained from the cluster calculations into the protein. A truncated protein model including the two close-lying biotin binding sites (abbreviated A and B) was used. Only monomer A is loaded with the artificial cofactor, leaving the biotin binding site of monomer B empty. This is justified by the observation that, upon adding 4

dx.doi.org/10.1021/cs400921n | ACS Catal. 2014, 4, 833−842

Table 1. Summary of the Computed Energies for All the Studied Cluster Mechanisms[a]

		Energy (kcal mol^{-1})						Distance (Å)	
mechanism	chiral.[a]	reactant	TS1	intermediate	TS2	product	TS2 frequency	C−H$^-$	Ir−H$^-$
H^-_{Ir}/H^+_{Ir}	*R*	0.0 (0.0)			26.1 (27.2)	2.9 (5.7)	−1048.8	1.46	1.79
	S	0.0 (0.0)			27.4 (25.9)	7.0 (7.0)	−1034.8	1.41	1.82
H^-_{Ir}/H^+_{Lys}	*R*	0.0 (0.0)	0.5 (−4.4)	−2.0 (−4.5)	10.2 (10.3)	−9.1 (−7.3)	−398.7	1.62	1.75
	S	0.0 (0.0)	0.6 (−2.2)	−1.3 (−3.8)	12.5 (12.4)	−3.9 (−4.5)	−343.4	1.62	1.73
H^-_{Ir}/H^+_{med}	R_{TSO}	0.0 (0.0)			12.0 (13.5)	−1.45 (0.4)	−325.5	1.55	1.74
	R_{TSN}	0.0 (0.0)			11.3 (12.4)	−13.0 (−8.8)	−325.0	1.69	1.74
	S_{TSO}	0.0 (0.0)			13.9 (18.0)	−0.8 (3.6)	−368.2	1.55	1.75
	S_{TSN}	0.0 (0.0)			8.9 (8.7)	−7.0 (−6.9)	−353.0	1.62	1.74

[a]Gibbs energies are given in parentheses. The distances between the transferring H and the heavy atoms and the frequencies associated to the reaction coordinate are given for each mechanism.

equivalents of artificial cofactor to tetrameric STREP, the enantioselectivity decreases noticeably.[10] The structure of the S112A STREP mutant obtained by Ward et al.[10] (PDB 3PK2) was selected as the protein scaffold. Docking was performed with the program GOLD (version 5.1)[56] and the Chemscore[57,58] scoring function. A covalent restraint, available in GOLD, was applied using N8 as the anchoring atom (Scheme 2a). The surrounding residues K121, L124, L110, and S88, which surrounded the organometallic moiety, were allowed flexibility using the Dunbrack rotameric library,[59] as implemented in GOLD. All structures were prepared as specified in the GOLD manual, using the UCSF Chimera interface.[60] An additional constraint corresponding to the reactive bonds was added, maintaining the first coordination sphere of the metal fixed. For the H^-_{Ir}/H^+_{Lys} mechanism, to ensure the suitable conformation of the lysine to act as a proton donor, a soft restraint was added between its Nζ (N12 in the cluster model; see Scheme 1) atom and the N_{imine} of the substrate. Twenty different solutions were generated for each run. The lowest energy solutions were selected as the starting point for hybrid QM/MM calculations. To relax clashes present on the docked structures, a few minimization steps were performed using the MMTK[61] minimizer, as implemented in the UCSF Chimera package with the AMBER forcefield.[62] The first coordination sphere of the metal was fixed to prevent a distortion of the transition state structure, because some nonstandard atoms are present.

QM/MM Calculations. For the QM/MM calculations, the two-layer ONIOM[63] approach implemented in Gaussian09 was applied using the electronic embedding scheme.[64] The QM region was treated using the same functional and the same basis set as those used for the cluster calculations. The MM region was treated with the Amber force field. Transition states and minima were validated by performing a frequency analysis at the same level of theory. The cyclic imine and all the atoms from the first coordination sphere of the metal, up to and including C9, were treated in the high-layer. For a better representation of the interactions between the substrate and the protein scaffold, the residues directly interacting with the substrate were also included in the high layer. For the H^-_{Ir}/H^+_{Lys} mechanism, this was the lysine acting as a proton donor. For the H^-_{Ir}/H^+_{med} TSO model, this was K121.A, while for the rest of the models belonging to that mechanism, it was K121.B. Lysine residues were included in the high region until the C_α atom. The rest of the system was included in the low layer. Residues L124.A, L124.B, L110.A, A112.A, K121.A, K121.B, and S88.A, as well as the entire (*R*)-[Cp*Ir(Biot-*p*-L)H] moiety and the substrate, were allowed flexibility during the calculation.

Enantiomeric Excess. The enantiomeric excess was calculated using the formula[65]

$$\%ee = \frac{1 - \exp^{\frac{-\Delta G^{\ddagger}_{R/S}}{RT}}}{1 + \frac{-\Delta G^{\ddagger}_{R/S}}{RT}} \times 100$$

where $\Delta G^{\ddagger}_{R/S}$ corresponds to the Gibbs energy difference obtained for the lowest energy transition states for (*R*)- and (*S*)-reduction products. The temperature was set to 298 K.

RESULTS

Preliminary Study on the Absolute Metal Configuration of [Cp*Ir(Biot-*p*-L)Cl] in S112A. Despite the exclusive presence of (*S*)-[Cp*Ir(Biot-*p*-L)Cl] in the X-ray structure of [Cp*Ir(Biot-*p*-L)Cl]⊂S112A,[10] the involvement of the (*R*)-enantiomer cannot be ruled out a priori. On the one hand, only the biotinylated ligand and the metal of the homogeneous catalyst are unambiguously resolved; the location of the Cp* and the chlorine is unclear. On the other hand, it is known that coordinately unsaturated pianostool 16-electron complexes readily racemise in solution.[66] Thus, a protein−ligand docking study was performed to probe which enantiomer of the catalyst precursor [Cp*Ir(Biot-*p*-L)Cl] is preferentially incorporated within streptavidin. Docking of both enantiomers was carried out and suggested: (i) a slightly better interaction of the (*S*)-enantiomer by 2 score units (5 kJ mol^{-1} in true Δ*G* binding energies), with respect to the (*R*)-one; (ii) significantly better overlap of the atoms that have been correctly resolved in the crystal structure for the (*S*)-enantiomer (RMSD = 1.0 Å) with the crystal structure than the (*R*)- (RMSD = 2.2 Å) − the (*R*) and the (*S*) enantiomers have their reactive faces pointing in opposite directions; (iii) highly solvent exposed conformation of the (*R*)-enantiomer. This is inconsistent with an impact of the proteic environment on the enantioselectivity of the reaction. These findings suggests that the protein selectively binds the (*S*)-[Cp*Ir(Biot-*p*-L)Cl] cofactor from the pseudo-racemic mixture (i.e., the (L)-biotin anchor is enantiopure) present in solution.[24] It thus appears that the second coordination sphere of the STREP-embedded artificial cofactor dictates the absolute configuration of the metal.

dx.doi.org/10.1021/cs400921n | ACS Catal. 2014, 4, 833−842

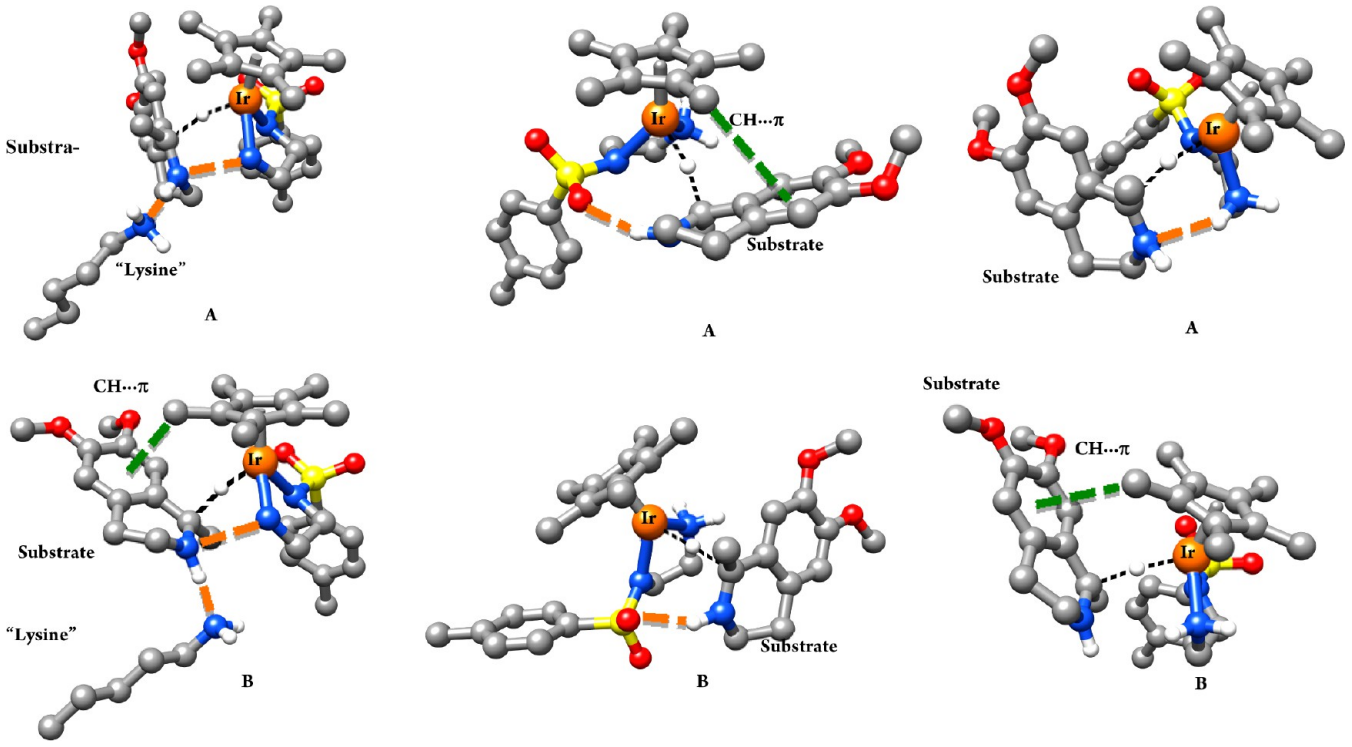

Figure 2. Transition state (TS) structures corresponding to the different mechanisms of reduction of the cyclic imine 1-methyl-6,7-dimethoxy-3,4-dihydroisoquinoline by the iridium catalyst (*R*)-[Cp*Ir(Biot-*p*-L)H]. (Left) H^-_{Ir}/H^+_{Lys} mechanism, *R* (A) and *S* (B) enantiomeric transition states. (Middle) TSO H^-_{Ir}/H^+_{med} mechanism; structures for the *R* (A) and *S* (B) enantiomeric transition states. (Right) TSN H^-_{Ir}/H^+_{med} mechanism; structures for the *R* (A) and *S* (B) enantiomeric transition states. The black dotted lines highlights the transfer of the hydride from the metal to the imine C, green dashed lines highlights C−H···π interactions, and orange segments represent hydrogen bonds.

Quantum Mechanical Study of Imine Hydrogenation. Since the (*S*)-[Cp*Ir(Biot-*p*-L)Cl] is the precursor of the (*R*)-[Cp*Ir(Biot-*p*-L)H] catalyst, all subsequent QM calculations on the cluster system were performed on an enantiopure model of this catalyst (see Scheme 2). Given the computed $pK_a = 6.35$ of the imine substrate,[67] we considered it both neutral and in the *N*-protonated form (hereafter imine and iminium, respectively). The hydride delivery was computed on both the *re* and *si* faces of the prochiral substrate.

For the imine, the reaction is expected to follow a ketone-like pathway, whereby both the proton and the hydride are transferred from the catalyst (H^-_{Ir}/H^+_{Ir} model; see Scheme 3). As summarized in Table 1, the activation energy for this process is very high (>25 kcal mol^{-1}). Hydride transfer to the iminium is much more favorable, as reflected in a significantly lower activation barrier (H^-_{Ir}/H^+_{med} models; see Table 1). This result is consistent with a recent report from Kacer and co-workers.[31] A transition state was located for both *re* and *si* delivery: these diastereomeric transition states differ in the mode of interaction between the imine and the catalyst. In some models, the protonated nitrogen of the substrate is hydrogen-bonded to one of the oxygen atoms of the sulfone-moiety (TSO models), whereas in others, the $-NH_2$ moiety of the first coordination sphere of the iridium is hydrogen-bonded to the imine nitrogen (TSN models). Further CH···π interactions stabilize the assembly (Figure 2). The lowest barrier was identified for the reduction of the *re* face of the substrate in the TSN orientation (~9 kcal mol^{-1}). This result differs from the conclusion of Kačer and co-workers who postulated that the polar interaction between the protonated substrate and the sulfone moiety of the Tos-dpen ligand (dpen = 1,2-dephenylethylene diamine) is the major driving force to guide the interaction between the catalyst and the substrate.[31] The discrepancies between the two studies may be traced back to differences in the computational approach, which include (i) the DFT functional (PBE in this work, B3LYP in Kačer et al.[31]), (ii) the solvent contributions (here optimizing an implicit solvent, while Kačer et al. performed gas-phase optimizations followed by implicit solvent single-point calculations) and (iii) the nature of the catalyst (here an {η^5-Cp*Ir}-based catalyst with an ethylenediamine ligand, while Kačer focused on a {η^6-*p*-cymeneRu} system with an 1,2-diphenylethylenediamine ligand).

Finally, we considered the possibility that an acidic group at the catalytic site could serve as a proton donor to the imine prior to the hydride transfer. A mimic of a lysine side chain (RNH_3^+) was included in the models featuring the neutral substrate (H^-_{Ir}/H^+_{Lys} models; see Scheme 3). We found that the transfer of a proton from the ammonium to the imine nitrogen is favorable and with a very small activation barrier (Table 1). These results suggest that the asynchronous mechanisms (i.e., protonation precedes hydride transfer) are energetically favorable compared to synchronous mechanism (operative for the ketone ATH). The proton source (water of close lying K121) does not play a determinant role in the corresponding (very low) activation barriers.[27] Next, we investigate the influence of the second coordination sphere imposed by STREP on the asynchronous pathways identified above as the most favorable.

Determination of Pseudo Transition State Structures in the (*R*)-[Cp*Ir(Biot-*p*-L)H]⊂S112A System. The transition state structures of the asynchronous pathways (H^-_{Ir}/

dx.doi.org/10.1021/cs400921n | ACS Catal. 2014, 4, 833−842

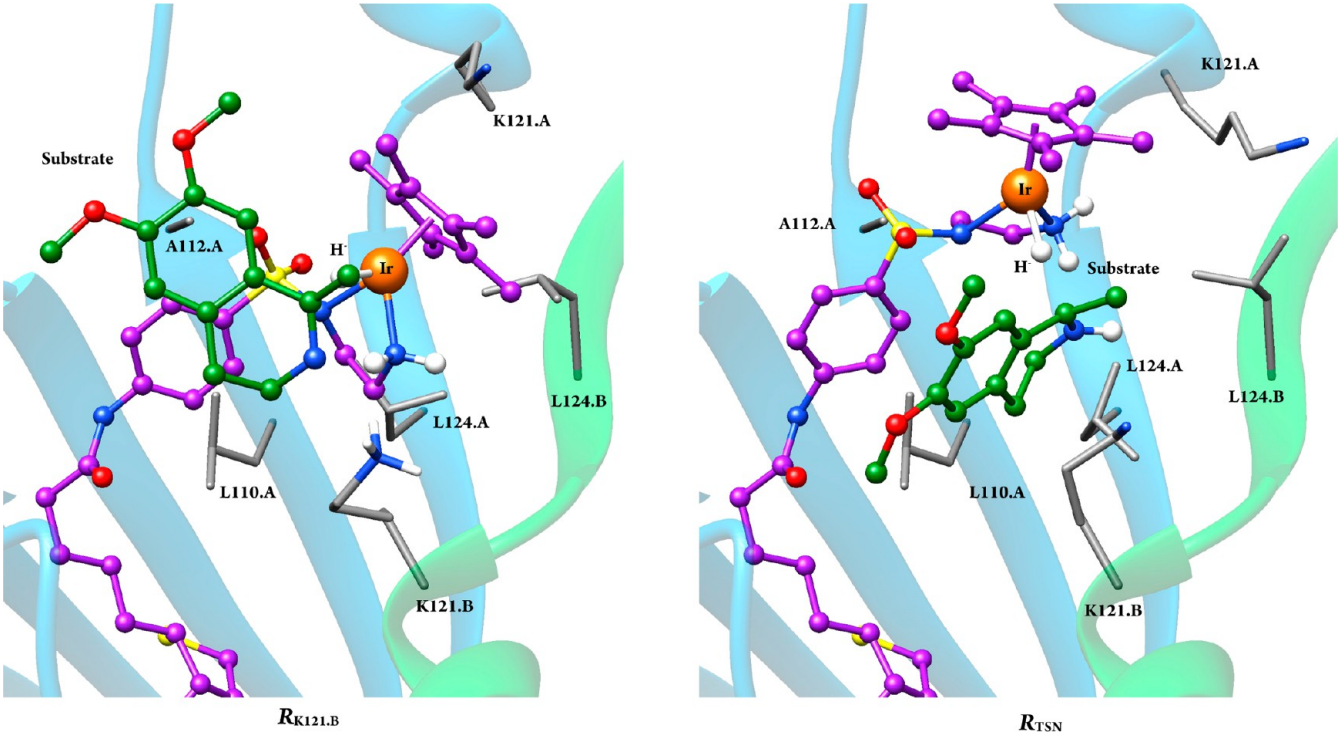

Figure 3. Lowest energy docking solutions from the H^-_{Ir}/H^+_{Lys} (left panel) and H^-_{Ir}/H^+_{med} (right panel) mechanisms.

H^+_{Med} and H^-_{Ir}/H^+_{Lys}) obtained from the cluster calculations were docked in the STREP S112A binding site. As catalytic experiments are routinely performed with 2 equivalents of cofactor per tetrameric STREP, only one transition state structure was docked in the protein dimer (in monomer A), leaving the opposite, but close-lying, biotin binding site B empty.

With regard to the H^-_{Ir}/H^+_{med} structures (four structures: (*R*)- and (*S*)-product pathways, TSN and TSO substrate orientations as defined in the previous section), the best docking solutions for R_{TSN}, R_{TSO}, and S_{TSN} (of similar affinities, see Table 1 in the Supporting Information) are consistent with the published structure of [Cp*Ir(Biot-*p*-L)Cl]⊂S112A: the $-SNCH_2CH_2NH_2$ moiety of the catalyst is embedded in the hydrophobic vestibule formed by the side chains of L110.A, A112.A, L124.A, L124.B and the backbone of S112.A, with the −NH group hydrogen-bonding the backbone carbonyl of K121.A, and the Cp* ligand interacting with the side chains of T114.A and K121.A. In the structures of R_{TSO} and S_{TSN}, the substrate is mostly interacting with hydrophobic residues of the neighboring peptide chain: L110.B, A112.B, the methyl of T114.B, the carbon chain of K121.B (without forming hydrogen bonds with the −OMe substituents), L124.B, and also L124.A. In the structure of R_{TSN}, the substrate interacts with L124.A (see Figure 3). The structure of S_{TSO} presents a distinct binding mode: the Cp* is buried in the hydrophobic pocket and the nonreactive face of the substrate points toward K121.A. In this orientation, the predicted binding energies are more favorable than for R_{TSN}, R_{TSO}, and S_{TSN}, suggesting a better complementarity between the transition state structure and the protein (Figure 3).

Concerning the H^-_{Ir}/H^+_{Lys} mechanism, in which the side chain of a lysine serves as a proton donor to the imine, we searched solutions for which K121 can interact with the imine nitrogen. Since there are two symmetry-related K121 residues in the biotin binding vestibule provided by monomers A and B, respectively, two docking solutions were computed for each pathway ((*R*)- and (*S*)-product pathways) (Figure 3). When K121.B is involved, solutions for both (*R*)- ($R_{K121.B}$) and (*S*)- ($S_{K121.B}$) pathways presents the Cp* ligand located at the solvent accessible region of the binding site. In $S_{K121.B}$, the −OMe groups interact with hydrophobic residues L110.A, A112.A, L124.A, W108.B, and L112.B. When K121.A is involved, the catalyst binding is similar for both (*R*)- and (*S*)-pathways (abbreviated $R_{K121.A}$ and $S_{K121.A}$ respectively), with the Cp* ligand located at the interface between the monomers. The substrate is highly solvent exposed and a polar contact with the corresponding lysine is the only interaction of the substrate with the protein scaffold.

The predicted binding affinities are ∼37 ChemScore units (see Table 1 in the Supporting Information). This suggests good complementarity of all transition state-like geometries of the catalyst and the substrate with the protein. Those of the H^-_{Ir}/H^+_{Lys} mechanism are, on average, better (39.4 ChemScore units) than the rest of the TSN and TSO transition states (36.3 ChemScore units). Analysis of the energetic deconvolution of the docking (see Table 1 in the Supporting Information) suggests that this energy difference is due to some clashes present in the latter, despite their apparent lipophilic complementarity. However, we hypothesized that QM/MM minimization might lead to a significant reduction in steric repulsion and thus influence the qualitative energetic ordering of these docked transition states. All these structures were thus scrutinized by QM/MM to investigate the impact of the protein scaffold on the energetics of the hydride transfer.

QM/MM Determination of the Enantiomeric Excess. The pseudo transition state structures—four for the H^-_{Ir}/H^+_{Lys} pathway and four for the H^-_{Ir}/H^+_{med} one—were used to initialize the search of true transition states computed by QM/MM. Once successfully located, the nearest minima on the

dx.doi.org/10.1021/cs400921n | *ACS Catal.* 2014, 4, 833−842

Table 2. Energies and Relevant Parameters from the Full Model QM/MM Calculations[a]

	Energy (kcal mol^{-1})				Distances	
model	reactant	TS	product	imaginary frequency	C−H$^-$	Ir−H$^-$
R_{TSO}	0.0 (0.0)	8.8 (9.1)	−17.8 (−13.7)	−333.6	1.52	1.77
R_{TSN}	0.0 (0.0)	0.7 (1.9)	−26.3 (−23.5)	−90.1	1.92	1.69
S_{TSO}	0.0 (0.0)	1.9 (3.2)	−2.9 (−1.1)	−147.0	1.65	1.73
S_{TSN}	0.0 (0.0)	13.3 (11.2)	−13.4 (−5.5)	−333.2	1.54	1.77
$R_{K121.A}$	0.0 (0.0)	21.7 (22.3)	2.5 (5.0)	−96.2	1.32	1.91
$S_{K121.A}$	0.0 (0.0)	17.6 (19.7)		−189.6	1.37	1.87
$R_{K121.B}$	0.0 (0.0)	23.3 (26.7)	10.1 (15.1)	−360.6	1.47	1.78
$S_{K121.B}$	0.0 (0.0)	27.5 (27.0)	13.3 (13.8)	−432.4	1.58	1.74

[a]The distances between the transferring H and the heavy atoms and the frequencies associated to the reaction coordinate are given for each mechanism (see Figure 2 for definition of TSO and TSN models). For K121.A, the proton source is lysine 121 from STREP monomer A; for K121.B, the proton source is lysine 121 from STREP monomer B.

potential energy surface were identified and used to compute the reaction energy profile.

The most favorable pathways were found for the H^-_{Ir}/H^+_{med} R_{TSN} and S_{TSO} mechanisms with $\Delta E^‡$ of 0.7 kcal mol^{-1} ($\Delta G^‡$ = 1.9 kcal mol^{-1}) and 1.9 kcal mol^{-1} ($\Delta G^‡$ = 3.2 kcal mol^{-1}), respectively (see Table 2). For these two mechanisms, this implies a decrease of the barrier close to 10 kcal mol^{-1}, compared to the cluster models. As the cluster calculations have been performed with a continuum solvent representation (something not possible at the current stage of the ONIOM implementation), we evaluated the contribution from the solvent by calculating the reaction barriers of the cluster models in the gas phase (see Table SI2 in the Supporting Information). Most of the reaction barriers display changes by <2 kcal mol^{-1}, compared to the continuum model, hence showing clearly that the decrease of the transition state energy for mechanism S_{TSO} is due to the interactions formed with the protein. For mechanism R_{TSN}, the QM/MM optimized structure shows the reacting center to be solvent excluded. Therefore, on the basis of the gas-phase cluster calculations, we conclude that the decrease of the transition state energy for this mechanism is due to both the interactions formed with the protein and the hydrophobic environment in which the reaction takes place. The two other H^-_{Ir}/H^+_{med} mechanisms, R_{TSO} and S_{TSN}, are characterized by energy barriers of 8.8 kcal mol^{-1} ($\Delta G^‡$ = 9.1 kcal mol^{-1}) and 13.3 kcal mol^{-1} ($\Delta G^‡$ = 11.2 kcal mol^{-1}), respectively. Relaxations to the product demonstrate that all these reactions are exothermic with ΔE_r values ranging from −2.9 kcal mol^{-1} to −26.0 kcal mol^{-1} (ΔG_r values from −1.1 kcal mol^{-1} to −23.5 kcal mol^{-1}). Compared to the pseudo transition state geometries from the dockings (see the previous section), the QM/MM-optimized transition states show small adaptations, the most noticeable of which is a relocation of K121.B in S_{TSN}, to interact with both the sulfone moiety of the catalyst and one methoxy group of the substrate.

Concerning the H^-_{Ir}/H^+_{Lys} pathway, the reaction proceeds in two successive steps with the transfer of a proton from a lysine residue preceding the transfer of the hydride from the metal center. The first step appears barrierless, as predicted with the cluster calculations. The second step has transition state energies varying from 17 kcal mol^{-1} to 27 kcal mol^{-1} (see Table 2). Compared to the pseudo transition state geometries, the QM/MM-optimized transition states exhibit minor adjustments, including the movement of K121.A and K121.B to maximize hydrogen-bond interactions with the O-methoxid group of the substrate and the rotation of the same group. Based on the energetic profiles obtained for the different mechanisms, we predict that the enzymatic activity of (*R*)-[Cp*Ir(Biot-*p*-L)H]⊂S112A proceed via either the R_{TSN} or S_{TSO} mechanisms. The difference of $\Delta G^‡$ between the two pathways is computed at 1.2 kcal mol^{-1} in favor of the (*R*)-amine. Although one should remain cautious in quantitative interpretations of *ee* from potential energy calculations, this leads to a predicted enantiomeric excess of 80% in favor of the (*R*)-salsolidine.[10] This value is in line with the experimental *ee* of 96% obtained at 278 K.[10]

DISCUSSION

In this study, we have relied on a range of modeling techniques to investigate and rationalize the molecular determinants at the origin of the enantioselectivity in the transfer hydrogenation of cyclic amines by the artificial enzyme [Cp*Ir(Biot-*p*-L)-Cl]⊂S112A. In the context of this class of artificial enzymes, the objective of modeling would be to predict the impact of protein mutations on the enantiomeric excess for a given transformation-substrate combination. Gaining such understanding requires to tackle several aspects of the reactivity, which include (i) the behavior of the organometallic catalyst bound to the protein, (ii) the recognition of the substrate, and (iii) the characterization of the chemical step itself. Addressing each of these issues by the most accurate computational techniques currently available would certainly be appropriate, but lengthy and computationally intensive. This approach is certainly too expensive for design purposes. The multistage strategy we present herein consists of three stages: (i) investigate the mechanism of the isolated organometallic catalyst, (ii) explore how the most favorable transition states fit into the host protein, and (iii) compute precise reaction barriers via QM/MM calculations on the entire system. A key requirement to unravel enantioselective mechanisms requires a detailed knowledge on how the organometallic catalyst and the prochiral substrate combine within the protein scaffold. To address this issue, we found it more convenient to determine first catalyst−substrate arrangements (actually, transition states), independently from the second coordination sphere contacts provided by the protein. These transition state structures were subsequently docked into the protein. Given the efficiency of docking calculations, we expect that this approach could be used to explore different protein variants, and thus guide the design of new artificial metaloenzymes. This strategy thus bears a resemblance to the work of Baker and Mayo, whereby a purely organic transition state is docked within a multitude of protein scaffolds to identify the most suitable host to stabilize the transition state.[6,39] However, it

dx.doi.org/10.1021/cs400921n | ACS Catal. 2014, 4, 833−842

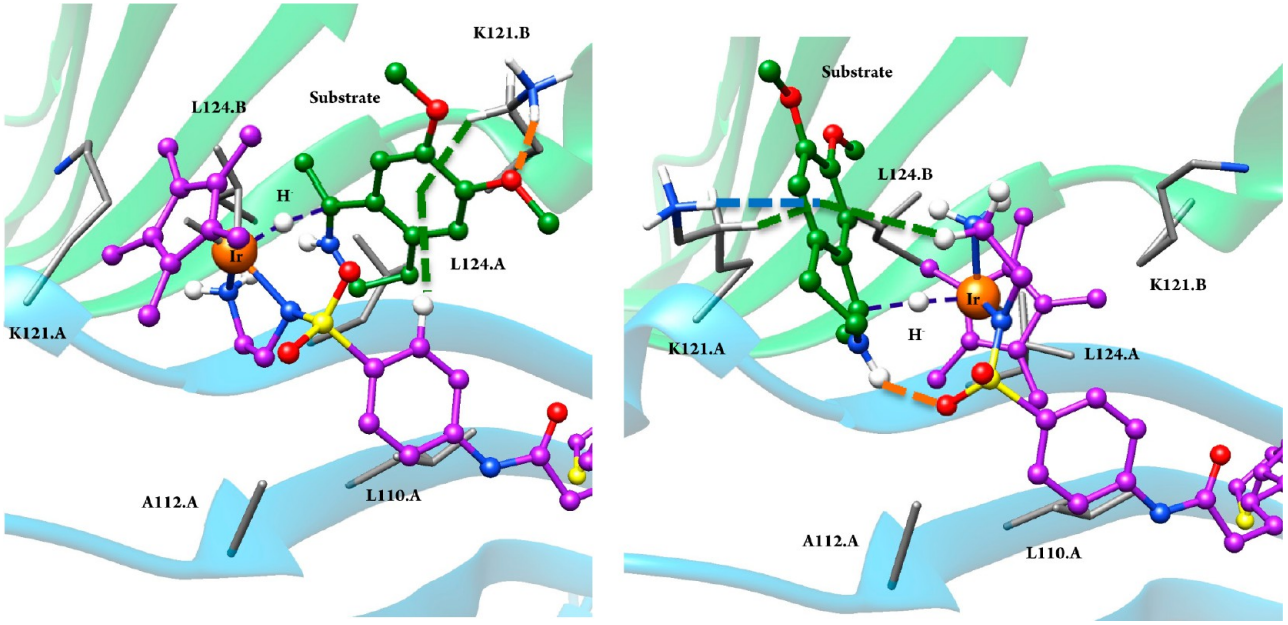

Figure 4. Lowest energy transition state structures from QM/MM calculations leading to the (*R*)-salsolidine (left panel) and (*S*)-salsolidine (right panel), respectively. Key interactions between the cofactor, the STREP, and the iminium substrate are highlighted: CH···π (green dashed lines), hydrogen-bond contacts (orange dashed lines), and cation···π (blue dashed lines).

heavily relies on QM/MM calculations to predict the final reactive models. This strategy is important to reach the energetic quality required for the rational design of enantioselective pathways. However, in the present case, no attempt has been made thus far to tailor the active site in a "lock-and-key" spirit.

As for any multilevel procedure, the quality of the results is conditioned by the accuracy of each individual technique. QM and QM/MM electronic structure calculations were performed within the DFT framework, which is the method of choice to tackle organometallic complexes. Nevertheless, and despite the ever-improving accuracy, DFT functionals do not yet approach chemical accuracy (<1 kcal mol^{-1}). The success of the DFT methodology applied to problems of enantioselectivity likely lies in the cancellation of errors which occurs when comparing different conformations of a given system.[65] Concerning the QM/MM calculations, solvation effects were neglected. Because of technical limitations, the continuum approach could not be applied, and adopting an explicit representation would have required proper sampling of the solvent degrees of freedom, considerably increasing the computational cost. Protein−ligand dockings are excellent tools to identify good and bad binding orientations but generally lacks the accuracy to discriminate between geometries with similar energies. Moreover, the atom types of the force fields used in these methods are optimized for purely organic ligands. Dealing with organometallic- and transition state-like structures require nonstandard handlings of the program.[68] At the different steps of the protocol, we take into account these limitations in order not to bias the search for the most favorable reaction mechanism. For example, only the mechanisms predicted by the QM cluster models to be substantially less stable than the others are selected for the subsequent steps of the procedure and all the possible orientations of the transition states in the protein resulting from the dockings were taken as starting points for the QM/MM computations (i.e., multiple lysine−substrate interactions).

The results obtained are encouraging. The computed enantiomeric excess is in good agreement with the experimental data, thus validating our approach. However, a note of caution is necessary here. Within the assumption that enantioselectivity is under kinetic control, an estimation of the enantiomeric excess requires the knowledge of the activation barriers for the diastereomeric reaction pathways. Given the exponential dependence of the enantiomeric excess on the difference between these barriers, the quality of the prediction is limited by the accuracy of the quantum chemical calculation.[65]

Apart from the actual value of the enantiomeric excess that we computed, the approach delineated herein provides valuable insight on the system. First, we note that three of the structures of the H^-_{Ir}/H^+_{med} pathway (R_{TSN}, S_{TSN}, and S_{TSO}) feature K121 interacting with the substrate, two of which (R_{TSN} and S_{TSN}) involve methoxy groups. In one of the structures of H^-_{Ir}/H^+_{Lys} pathway, we found the other K121 interacting with one methoxy group of the substrate. It is thus apparent that K121 is a key residue involved in the stabilization of the transition state. Indeed, experimentally it was found that selectivity is considerably lowered for the S112A−K121T variant with (*R*)-salsolidine produced in 52% *ee*.[10] This finding is also consistent with the observation that, upon deletion of the methoxy groups of the substrate, which according to our computations interact with K121, selectivity is decreased significantly: reduction of 1-methyl-3,4-dihydroisoquinoline by [Cp*Ir(Biot-*p*-L)Cl]⊂S112A yield (*R*)-1-methylisoquinoline in 50% *ee* (compared to 93% *ee* for salsolidine).[69]

Second, four of the eight computed transition state structures feature the organometallic moiety in a conformation similar to the published X-ray structure of [Cp*Ir(Biot-*p*-L)Cl]⊂S112A. The others are related by some degree of rotation of the Ir complex along the O_2S-N axis, with S_{TSO} featuring ∼180° rotation of the pianostool moiety, which is buried in the protein vestibule. A similar rotation along the O_2S-N bond within the biotin-binding vestibule was reported previously for [(C_6H_6)-Ru(Biot-*p*-L)Cl]⊂S112K.[14] Given that all these binding modes

dx.doi.org/10.1021/cs400921n | *ACS Catal.* 2014, 4, 833−842

have similar ChemScore affinities, these findings highlight a considerable degree of flexibility of the organometallic complex within the binding site.

Third, the protein has a dramatic impact on the activation energy, lowering the barrier by as much as 10 kcal mol^{-1} for the lowest energy mechanisms R_{TSN} and S_{TSO}. The transition states that experience the largest stabilization feature an increase of the C···hydride distance: 1.9 Å for the R_{TSN} and 1.65 Å for the S_{TSO}, versus 1.69 Å and 1.55 Å in the cluster models, respectively. The computations indicate that the protein environment does not alter the mechanism of the ATH of cyclic imines, which is found to be the same as that described for the cluster models. This mechanism is in agreement with the experimental results obtained by Wills and co-workers.[27,70] It should be stated that the stabilization of the protein environment cannot be traced back to a unique interaction between the catalyst/protein/substrate triad. Nonetheless, as observed in the docking, there is a significant contribution from the hydrophobicity of the pocket (mainly the two L124 from both monomers in R_{TSN} and T114.A, A112.A, and K112.A in S_{TSO}, Figure 4) as well as from polar interactions with K112.B (for R_{TSN}) and K112.A (for S_{TSO}).

CONCLUSION

The integrated computational approach that we have pursued in this study has allowed us to disclose the molecular interactions responsible for the enantioselective reduction of cyclic imines by the artificial transfer hydrogenase (*R*)-[Cp*Ir(Biot-*p*-L)Cl]⊂S112A. It sheds light onto the homogeneous and enzymatic process by which Noyori-like catalysts reduce imines and illustrate the complexity to predict the molecular behavior of non-natural biometallic hybrids. This study shows the role of asymmetric second coordination sphere environment provided by the protein in dictating the enantioselectivity of the reaction. In particular, it demonstrates that K121 stabilizes the orientation of the substrate in the lowest energy transition state by simultaneously forming a hydrogen bond with its −OMe group and a C−H···π interaction.

The procedure presented is computationally efficient and provides detailed structural information, one of the key elements for the rational optimization of artificial enzymes. Based on realistic but approximate "pseudo transition state" structures, the strategy could be adapted to any biological catalysts for which the identification of reactive paths is troublesome. It could be particularly valuable for systems where a large conformational space must be explored to isolate real-size transition state structures. This includes mechanism involving a molecular triad (i.e., those involving coenzymes or cosubstrates), as well as those with important flexibility in their binding site.

ASSOCIATED CONTENT

Supporting Information

Additional tables and geometries of the cluster models are provided as Supporting Information. This material is available free of charge via the Internet at http://pubs.acs.org.

AUTHOR INFORMATION

Corresponding Author

*E-mail: jeandidier.marechal@uab.cat.

Author Contributions

The manuscript was written through contributions of all authors.

Notes

The authors declare no competing financial interest.

ACKNOWLEDGMENTS

Financial support from the Spanish Ministerio de Economia y Competitividad (Project CTQ2011-23336) is acknowledged. V.M.R. is grateful to the Spanish MINECO for a FPI Fellowship.

REFERENCES

(1) Ringenberg, M. R.; Ward, T. R. *Chem. Commun.* **2011**, *47*, 8470−8476.
(2) Rosati, F.; Roelfes, G. *ChemCatChem* **2010**, *2*, 916−927.
(3) Roelfes, G. *Mol. Biosyst.* **2007**, *3*, 126−135.
(4) Kiss, G.; Röthlisberger, D.; Baker, D.; Houk, K. N. *Protein Sci.* **2010**, *19*, 1760−1773.
(5) Ueno, T.; Yokoi, N.; Unno, M.; Matsui, T.; Tokita, Y.; Yamada, M.; Ikeda-Saito, M.; Nakajima, H.; Watanabe, Y. *Proc. Natl. Acad. Sci. U. S. A.* **2006**, *103*, 9416−9421.
(6) Khare, S. D.; Kipnis, Y.; Greisen, P. J.; Takeuchi, R.; Ashani, Y.; Goldsmith, M.; Song, Y.; Gallaher, J. L.; Silman, I.; Leader, H.; Sussman, J. L.; Barry, L. S.; Tawfik, D. S.; Baker, D. *Nat. Chem. Biol.* **2012**, *8*, 294−300.
(7) Hyster, T. K.; Knörr, L.; Ward, T. R.; Rovis, T. *Science* **2012**, *338*, 500−503.
(8) Allard, M.; Dupont, C.; Muñoz Robles, V.; Doucet, N.; Lledós, A.; Maréchal, J.-D.; Urvoas, A.; Mahy, J.-P.; Ricoux, R. *ChemBioChem* **2012**, *13*, 240−251.
(9) Esmieu, C.; Cherrier, M. V; Amara, P.; Girgenti, E.; Marchi-Delapierre, C.; Oddon, F.; Iannello, M.; Jorge-Robin, A.; Cavazza, C.; Ménage, S. *Angew. Chem., Int. Ed.* **2013**, *52*, 3922−3925.
(10) Dürrenberger, M.; Heinisch, T.; Wilson, Y. M.; Rossel, T.; Nogueira, E.; Knörr, L.; Mutschler, A.; Kersten, K.; Zimbron, M. J.; Pierron, J.; Schirmer, T.; Ward, T. R. *Angew. Chem., Int. Ed.* **2011**, *50*, 3026−3029.
(11) Robles, V. M.; Ortega-Carrasco, E.; Fuentes, E. G.; Lledós, A.; Maréchal, J.-D. *Faraday Discuss.* **2011**, *148*, 137−159.
(12) Ueno, T.; Koshiyama, T.; Abe, S.; Yokoi, N.; Ohashi, M.; Nakajima, H.; Watanabe, Y. *J. Organomet. Chem.* **2007**, *692*, 142−147.
(13) Carey, J. R.; Ma, S. K.; Pfister, T. D.; Garner, D. K.; Kim, H. K.; Abramite, J. a; Wang, Z.; Guo, Z.; Lu, Y. *J. Am. Chem. Soc.* **2004**, *126*, 10812−10813.
(14) Creus, M.; Pordea, A.; Rossel, T.; Sardo, A.; Letondor, C.; Ivanova, A.; Letrong, I.; Stenkamp, R. E.; Ward, T. R. *Angew. Chem., Int. Ed.* **2008**, *47*, 1400−1404.
(15) Wilson, M. E.; Whitesides, G. M. *J. Am. Chem. Soc.* **1978**, *100*, 306−307.
(16) Lin, C.-C.; Lin, C.-W.; Chan, A. S. C. *Tetrahedron: Asymmetry* **1999**, *10*, 1887−1893.
(17) Reetz, M. T.; Peyralans, J. J.-P.; Maichele, A.; Fu, Y.; Maywald, M. *Chem. Commun.* **2006**, 4318−4320.
(18) Letondor, C.; Pordea, A.; Humbert, N.; Ivanova, A.; Mazurek, S.; Novic, M.; Ward, T. R. *J. Am. Chem. Soc.* **2006**, *128*, 8320−8328.
(19) Zimbron, J. M.; Heinisch, T.; Schmid, M.; Hamels, D.; Nogueira, E. S.; Schirmer, T.; Ward, T. R. *J. Am. Chem. Soc.* **2013**, *135*, 5384−5388.
(20) Ward, T. R. *Acc. Chem. Res.* **2011**, *44*, 47−57.
(21) Lo, C.; Ringenberg, M. R.; Gnandt, D.; Wilson, Y.; Ward, T. R. *Chem. Commun.* **2011**, *47*, 12065−12067.
(22) Thomas, C. M.; Letondor, C.; Humbert, N.; Ward, T. R. *J. Organomet. Chem.* **2005**, *690*, 4488−4491.
(23) Kokubo, T.; Sugimoto, T.; Uchida, T.; Tanimoto, S.; Okano, M. *J. Chem. Soc., Chem. Commun.* **1983**, 769−770.

(24) Loosli, A.; Rusbandi, U. E.; Gradinaru, J.; Bernauer, K.; Schlaepfer, C. W.; Meyer, M.; Mazurek, S.; Novic, M.; Ward, T. R. *Inorg. Chem.* **2006**, *45*, 660−668.
(25) Heinisch, T.; Langowska, K.; Tanner, P.; Reymond, J.-L.; Meier, W.; Palivan, C.; Ward, T. R. *ChemCatChem* **2013**, *5*, 720−723.
(26) Yamakawa, M.; Yamada, I.; Noyori, R. *Angew. Chem., Int. Ed.* **2001**, *40*, 2818−2821.
(27) Martins, J. E. D.; Clarkson, G. J.; Wills, M. *Org. Lett.* **2009**, *11*, 847−850.
(28) Fabrello, A.; Bachelier, A.; Urrutigoïty, M.; Kalck, P. *Coord. Chem. Rev.* **2010**, *254*, 273−287.
(29) Hopmann, K. H.; Bayer, A. *Organometallics* **2011**, *30*, 2483−2497.
(30) Pablo, Ó.; Guijarro, D.; Kovács, G.; Lledós, A.; Ujaque, G.; Yus, M. *Chem.—Eur. J.* **2012**, *18*, 1969−1983.
(31) Václavík, J.; Kuzma, M.; Přech, J.; Kačer, P. *Organometallics* **2011**, *30*, 4822−4829.
(32) Åberg, J. B.; Samec, J. S. M.; Bäckvall, J. E. *Chem. Commun.* **2006**, *70*, 2771−2773.
(33) Zhu, Y.; Fan, Y.; Burgess, K. *J. Am. Chem. Soc.* **2010**, *132*, 6249−6253.
(34) Althoff, E. A.; Wang, L.; Jiang, L.; Giger, L.; Lassila, J. K.; Wang, Z.; Smith, M.; Hari, S.; Kast, P.; Herschlag, D.; Hilvert, D.; Baker, D. *Protein Sci.* **2012**, *21*, 717−726.
(35) Richter, F.; Blomberg, R.; Khare, S. D.; Kiss, G.; Kuzin, A. P.; Smith, A. J. T.; Gallaher, J.; Pianowski, Z.; Helgeson, R. C.; Grjasnow, A.; Xiao, R.; Seetharaman, J.; Su, M.; Vorobiev, S.; Lew, S.; Forouhar, F.; Kornhaber, G. J.; Hunt, J. F.; Montelione, G. T.; Tong, L.; Houk, K. N.; Hilvert, D.; Baker, D. *J. Am. Chem. Soc.* **2012**, *134*, 16197−16206.
(36) Bolon, D. N.; Mayo, S. L. *Proc. Natl. Acad. Sci. U. S. A.* **2001**, *98*, 14274−14279.
(37) Malakauskas, S. M.; Mayo, S. L. *Nat. Struct. Biol.* **1998**, *5*, 470−475.
(38) Dahiyat, B. I.; Mayo, S. L. *Science* **1997**, *278*, 82−87.
(39) Privett, H. K.; Kiss, G.; Lee, T. M.; Blomberg, R.; Chica, R. A.; Thomas, L. M.; Hilvert, D.; Houk, K. N.; Mayo, S. L. *Proc. Natl. Acad. Sci. U. S. A.* **2011**, *109*, 3790−3795.
(40) Blomberg, R.; Kries, H.; Pinkas, D. M.; Mittl, P. R. E.; Grütter, M. G.; Privett, H. K.; Mayo, S. L.; Hilvert, D. *Nature* **2013**, DOI: 10.103/nature12623.
(41) Ke, Z.; Abe, S.; Ueno, T.; Morokuma, K. *J. Am. Chem. Soc.* **2012**, *134*, 15418−29.
(42) Lind, M. E. S.; Himo, F. *Angew. Chem., Int. Ed.* **2013**, *125*, 4661−4665.
(43) Polyak, I.; Reetz, M. T.; Thiel, W. *J. Am. Chem. Soc.* **2012**, *134*, 2732−2741.
(44) Polyak, I.; Reetz, M. T.; Thiel, W. *J. Phys. Chem. B* **2013**, *117*, 4993−5001.
(45) Bocola, M.; Otte, N.; Jaeger, K. E.; Reetz, M. T.; Thiel, W. *ChemBioChem* **2004**, *5*, 214−223.
(46) Reetz, M. T.; Puls, M.; Carballeira, J. D.; Vogel, A.; Jaeger, K.-E.; Eggert, T.; Thiel, W.; Bocola, M.; Otte, N. *ChemBioChem* **2007**, *8*, 106−12.
(47) Perdew, J.; Burke, K.; Ernzerhof, M. *Phys. Rev. Lett.* **1996**, *77*, 3865−3868.
(48) Perdew, J. P.; Ernzerhof, M.; Burke, K. *J. Chem. Phys.* **1996**, *105*, 9982−9985.
(49) Frisch, M. J.; Trucks, G. W.; Schlegel, H. B.; Scuseria, G. E.; Robb, M. A.; Cheeseman, J. R.; Scalmani, G.; Barone, V.; Mennucci, B.; Petersson, G. A.; Nakatsuji, H.; Caricato, M.; Li, X.; Hratchian, H. P.; Izmaylov, A. F.; Bloino, J.; Zheng, G.; Sonnenberg, J. L.; Hada, M.; Ehara, M.; Toyota, K.; Fukuda, R.; Hasegawa, J.; Ishida, M.; Nakajima, T.; Honda, Y.; Kitao, O.; Nakai, H.; Vreven, T.; Montgomery, J. A.; Jr.; Peralta, J. E.; Ogliaro, F.; Bearpark, M.; Heyd, J. J.; Brothers, E.; Kudin, K. N.; Staroverov, V. N.; Kobayashi, R.; Normand, J.; Raghavachari, K.; Rendell, A.; Burant, J. C.; Iyengar, S. S.; Tomasi, J.; Cossi, M.; Rega, N.; Millam, J. M.; Klene, M.; Knox, J. E.; Cross, J. B.; Bakken, V.; Adamo, C.; Jaramillo, J.; Gomperts, R.; Stratmann, R. E.; Yazyev, O.; Austin, A. J.; Cammi, R.; Pomelli, C.; Ochterski, J. W.; Martin, R. L.; Morokuma, K.; Zakrzewski, V. G.; Voth, G. A.; Salvador, P.; Dannenberg, J. J.; Dapprich, S.; Daniels, A. D.; Farkas, Ö.; Foresman, J. B.; Ortiz, J. V.; Cioslowski, J.; Fox, D. J. *Gaussian 09, Revision A.1*; Gaussian: Wallingford, CT, 2009.
(50) Weigend, F.; Ahlrichs, R. *Phys. Chem. Chem. Phys.* **2005**, *7*, 3297−3305.
(51) Hehre, W. J. *J. Chem. Phys.* **1972**, *56*, 2257−2261.
(52) Klamt, A.; Schüürmann, G. *J. Chem. Soc., Perkin Trans. 2* **1993**, 799−805.
(53) Andzelm, J.; Kölmel, C.; Klamt, A. *J. Chem. Phys.* **1995**, *103*, 9312−9320.
(54) Barone, V.; Cossi, M. *J. Phys. Chem. A* **1998**, *102*, 1995−2001.
(55) Cossi, M.; Rega, N.; Scalmani, G.; Barone, V.; Chimica, D.; Ii, F.; Angelo, C. M. S. *J. Comput. Chem.* **2003**, *24*, 669−681.
(56) Verdonk, M. L.; Cole, J. C.; Hartshorn, M. J.; Murray, C. W.; Taylor, R. D. *Proteins* **2003**, *52*, 609−623.
(57) Eldridge, M. D.; Murray, C. W.; Auton, T. R.; Paolini, G. V.; Mee, R. P. *J. Comput. Aided. Mol. Des.* **1997**, *11*, 425−445.
(58) Baxter, C. A.; Murray, C. W.; Clark, D. E.; Westhead, D. R.; Eldridge, M. D. *Proteins* **1998**, *33*, 367−382.
(59) Chase, F.; Avenue, B. *Curr. Opin. Struct. Biol.* **2002**, *12*, 431−440.
(60) Pettersen, E. F.; Goddard, T. D.; Huang, C. C.; Couch, G. S.; Greenblatt, D. M.; Meng, E. C.; Ferrin, T. E. *J. Comput. Chem.* **2004**, *25*, 1605−1612.
(61) Hinsen, K. *J. Comput. Chem.* **2000**, *21*, 79−85.
(62) Cornell, W. D.; Cieplak, P.; Bayly, C. I.; Gould, I. R.; Merz, K. M.; Ferguson, D. M.; Spellmeyer, D. C.; Fox, T.; Caldwell, J. W.; Kollman, P. A. *J. Am. Chem. Soc.* **1995**, *117*, 5179−5197.
(63) Byun, K. S.; Morokuma, K. *J. Mol. Struct. THEOCHEM* **1999**, *461−462*, 1−21.
(64) Bakowies, D.; Thiel, W. *J. Phys. Chem.* **1996**, *3654*, 10580−10594.
(65) Balcells, D.; Maseras, F. *New J. Chem.* **2007**, *31*, 333−343.
(66) Ward, T. R.; Schafer, O.; Daul, C.; Hofmann, P. *Organometallics* **1997**, *16*, 3207−3215.
(67) *ChemAxon Marvin*, 2013 (http://www.chemaxon.com).
(68) Ortega Carrasco, E.; Lledós, A.; Maréchal, J.-D. *J. Comput. Chem.* **2013**, *35*, 192−198.
(69) Köhler, V.; Wilson, Y. M.; Dürrenberger, M.; Ghislieri, D.; Churakova, E.; Quinto, T.; Knörr, L.; Häussinger, D.; Hollmann, F.; Turner, N. J.; Ward, T. R. *Nat. Chem.* **2013**, *5*, 93−99.
(70) Soni, R.; Cheung, F. K.; Clarkson, G. C.; Martins, J. E. D.; Graham, M. A.; Wills, M. *Org. Biomol. Chem.* **2011**, *9*, 3290−3294.